Metadata of the article that will be visualized in OnlineFirst

1	Article Title	**MR volumetric assessment of endolymphatic hydrops**	
2	Article Sub- Title		
3	Article Copyright - Year	**European Society of Radiology 2014 (This will be the copyright line in the final PDF)**	
4	Journal Name	European Radiology	
5	Corresponding Author	Family Name	**Gürkov**
6		Particle	
7		Given Name	**R.**
8		Suffix	
9		Organization	University of Munich
10		Division	German Centre for Vertigo and Balance Disorders, Grosshadern Medical Centre
11		Address	Marchioninistr. 15, Munich, 81377, Germany
12		Organization	University of Munich
13		Division	Department of Otorhinolaryngology Head and Neck Surgery, Grosshadern Medical Centre
14		Address	Marchioninistr. 15, Munich 81377, Germany
15		e-mail	rguerkov@med.uni-muenchen.de
16	Author	Family Name	**Berman**
17		Particle	
18		Given Name	**A.**
19		Suffix	
20		Organization	University of Munich
21		Division	Department of Otorhinolaryngology Head and Neck Surgery, Grosshadern Medical Centre
22		Address	Marchioninistr. 15, Munich 81377, Germany
23		Organization	University of Munich
24		Division	German Centre for Vertigo and Balance Disorders, Grosshadern Medical Centre
25		Address	Marchioninistr. 15, Munich, 81377, Germany
26		e-mail	
27	Author	Family Name	**Dietrich**
28		Particle	

29		Given Name	**O.**
30		Suffix	
31		Organization	University of Munich
32		Division	Department of Otorhinolaryngology Head and Neck Surgery, Grosshadern Medical Centre
33		Address	Marchioninistr. 15, Munich 81377, Germany
34		Organization	University of Munich
35		Division	German Centre for Vertigo and Balance Disorders, Grosshadern Medical Centre
36		Address	Marchioninistr. 15, Munich, 81377, Germany
37		e-mail	
38		Family Name	**Flatz**
39		Particle	
40		Given Name	**W.**
41		Suffix	
42	Author	Organization	University of Munich
43		Division	Institute of Clinical Radiology, Grosshadern Medical Centre
44		Address	Marchioninistr. 15, Munich 81377, Germany
45		e-mail	
46		Family Name	**Jerin**
47		Particle	
48		Given Name	**C.**
49		Suffix	
50		Organization	University of Munich
51	Author	Division	Department of Otorhinolaryngology Head and Neck Surgery, Grosshadern Medical Centre
52		Address	Marchioninistr. 15, Munich 81377, Germany
53		Organization	University of Munich
54		Division	German Centre for Vertigo and Balance Disorders, Grosshadern Medical Centre
55		Address	Marchioninistr. 15, Munich, 81377, Germany
56		e-mail	
57		Family Name	**Krause**
58		Particle	
59	Author	Given Name	**E.**
60		Suffix	
61		Organization	University of Munich

62		Division	Department of Otorhinolaryngology Head and Neck Surgery, Grosshadern Medical Centre
63		Address	Marchioninistr. 15, Munich 81377, Germany
64		Organization	University of Munich
65		Division	German Centre for Vertigo and Balance Disorders, Grosshadern Medical Centre
66		Address	Marchioninistr. 15, Munich, 81377, Germany
67		e-mail	
68		Family Name	**Keeser**
69		Particle	
70		Given Name	**D.**
71		Suffix	
72		Organization	University of Munich
73		Division	Institute of Clinical Radiology, Grosshadern Medical Centre
74		Address	Marchioninistr. 15, Munich 81377, Germany
75	Author	Organization	University of Munich
76		Division	German Centre for Vertigo and Balance Disorders, Grosshadern Medical Centre
77		Address	Marchioninistr. 15, Munich, 81377, Germany
78		Organization	University of Munich
79		Division	Department of Psychiatry and Psychotherapy, Innenstadtkliniken Medical Centre
80		Address	Nussbaumstraße 7, Munich 80336, Germany
81		e-mail	
82		Family Name	**Ertl-Wagner**
83		Particle	
84		Given Name	**B.**
85		Suffix	
86	Author	Organization	University of Munich
87		Division	Institute of Clinical Radiology, Grosshadern Medical Centre
88		Address	Marchioninistr. 15, Munich 81377, Germany
89		e-mail	
90		Received	5 April 2014
91	Schedule	Revised	4 August 2014
92		Accepted	26 August 2014
93	Abstract		

94 Keywords separated by ' - ' Menière's disease - Endolymphatic hydrops - Magnetic resonance imaging - Drug administration routes - Image analysis

95 Foot note information

R. Gürkov and A. Berman equally contributed as First Authors

D. Keeser and B. Ertl-Wagner equally contributed as Last Authors

The online version of this article (doi:10.1007/s00330-014-3414-4) contains supplementary material, which is available to authorized users.

Electronic supplementary material

ESM 1
Volume rendering of right inner ear with moderate endolymphatic hydrops. Perilymph space is colored cyan, endolymph space is colored red. Cochlear endolymphatic space is most dilated in the apical region, whereas in the basal turn and ductus reuniens it appears not dilated. Vestibular endolymphatic space is moderately dilated, and there is no herniation into the non-ampullated crura of the semicircular canals. Rotation around yaw axis (Video 1) and around pitch axis (Video 2). (AVI 4223 kb)

Eur Radiol
DOI 10.1007/s00330-014-3414-4

HEAD AND NECK

MR volumetric assessment of endolymphatic hydrops

R. Gürkov · A. Berman · O. Dietrich · W. Flatz · C. Jerin · E. Krause · D. Keeser · B. Ertl-Wagner

Received: 5 April 2014 / Revised: 4 August 2014 / Accepted: 26 August 2014

Abstract
Objectives We aimed to volumetrically quantify endolymph and perilymph spaces of the inner ear in order to establish a methodological basis for further investigations into the pathophysiology and therapeutic monitoring of Menière's disease.
Methods Sixteen patients (eight females, aged 38–71 years) with definite unilateral Menière's disease were included in this study. Magnetic resonance (MR) cisternography with a T2-SPACE sequence was combined with a Real reconstruction inversion recovery (Real-IR) sequence for delineation of inner ear fluid spaces. Machine learning and automated local thresholding segmentation algorithms were applied for three-dimensional (3D) reconstruction and volumetric quantification of endolymphatic hydrops. Test–retest reliability was assessed by the intra-class coefficient; correlation of cochlear endolymph volume ratio with hearing function was assessed by the Pearson correlation coefficient.
Results Endolymph volume ratios could be reliably measured in all patients, with a mean (range) value of 15 % (2–25) for the cochlea and 28 % (12–40) for the vestibulum. Test-retest reliability was excellent, with an intra-class coefficient of 0.99. Cochlear endolymphatic hydrops was significantly correlated with hearing loss (r=0.747, p=0.001).
Conclusions MR imaging after local contrast application and image processing, including machine learning and automated local thresholding, enable the volumetric quantification of endolymphatic hydrops. This allows for a quantitative assessment of the effect of therapeutic effects on endolymphatic hydrops.
Key Points
- *Endolymphatic hydrops is the pathological hallmark of Menière's disease.*
- *Endolymphatic hydrops can be visualized by locally enhanced ultra-high-resolution MR imaging.*
- *Computer-aided image processing enables quantification of endolymphatic hydrops.*
- *Endolymphatic hydrops correlates with hearing loss in patients with Menière's disease.*
- *Therapeutic trials in Menière's disease can be monitored with this quantitative approach.*

Keywords Menière's disease · Endolymphatic hydrops · Magnetic resonance imaging · Drug administration routes · Image analysis

Introduction

Menière's disease (MD) is a disorder of inner ear homeostasis causing vertigo, hearing loss and tinnitus in about 0.2–0.5 %

R. Gürkov and A. Berman equally contributed as First Authors

D. Keeser and B. Ertl-Wagner equally contributed as Last Authors

Electronic supplementary material The online version of this article (doi:10.1007/s00330-014-3414-4) contains supplementary material, which is available to authorized users.

R. Gürkov · A. Berman · O. Dietrich · C. Jerin · E. Krause
Department of Otorhinolaryngology Head and Neck Surgery, Grosshadern Medical Centre, University of Munich, Marchioninistr. 15, 81377 Munich, Germany

W. Flatz · D. Keeser · B. Ertl-Wagner
Institute of Clinical Radiology, Grosshadern Medical Centre, University of Munich, Marchioninistr. 15, 81377 Munich, Germany

R. Gürkov (✉) · A. Berman · O. Dietrich · C. Jerin · E. Krause · D. Keeser
German Centre for Vertigo and Balance Disorders, Grosshadern Medical Centre, University of Munich, Marchioninistr. 1581377 Munich, Germany
e-mail: rguerkov@med.uni-muenchen.de

D. Keeser
Department of Psychiatry and Psychotherapy, Innenstadtkliniken Medical Centre, University of Munich, Nussbaumstraße 7, 80336 Munich, Germany

of the general population [1, 2]. Its pathological hallmark is a distension of the endolymphatic space, termed endolymphatic hydrops (ELH) [3, 4], resulting in an increased proportion of endolymph (EL) within the total fluid space of the inner ear. The diagnosis of Menière's disease is based upon the typical clinical syndrome and the demonstration of ELH [5]. Since the latter could previously be obtained only by histological post-mortem examination, clinical practitioners and researchers had to rely upon the clinical manifestations alone in order to establish the diagnosis of MD.

After Zou et al. first reported separate visualization of endolymph and perilymph spaces in living humans by magnetic resonance (MR) imaging [6], Nakashima et al. [7] first provided evidence for the feasibility of visualization of ELH in living MD patients by locally enhanced inner ear MR imaging (LEIM). Using a three-dimensional (3D) fluid-attenuated inversion recovery (FLAIR) sequence, a high signal intensity within the perilymph was achieved after application of gadolinium-based contrast medium (GBCM) into the middle ear. This method could separate perilymph from both endolymph and bone, but not endolymph from bone. Naganawa et al. [8] then introduced the 3D Real reconstruction inversion recovery (Real-IR), which was able to differentiate endolymph, perilymph and surrounding bone for the first time by a single sequence. More recent work used modifications of these sequences to demonstrate endolymphatic hydrops even after single dose i.v. administration of GBCM [9].

So far, however, in vivo measurements of ELH have only led to semi-quantitative and subjective data, based on the 2D or 3D manual segmentation of endolymph and perilymph spaces [8, 10–12]. The objective and volumetric quantification of the endolymph / total fluid space (EL/TFS) ratio in patients with MD is, however, a necessary next step to allow systematic pathophysiological and therapeutic studies of ELH in MD. Several factors make an objective volumetric assessment of inner ear fluid spaces a challenging task: (1) Intra-tympanic GBCM application achieves a higher signal intensity than does i.v. application, but the signal distribution within the inner ear is less uniform [13]. An uneven signal distribution impedes precise automated segmentation using a single threshold value. (2) The Real-IR sequence provides a very good contrast between endolymph and perilymph. However, the border between perilymph and surrounding bone is too fuzzy for precise automated segmentation. We aimed to volumetrically quantify endolymph and perilymph spaces of the inner ear in order to establish a methodological basis for further investigations into the pathophysiology of Menière's disease and to potentially monitor future therapeutic approaches.

Methods

Subjects

This prospective study was approved by the local Institutional Review Board / University Ethics Committee (Protocol No. 093-09). All patients provided oral and written informed consent. Sixteen consecutive patients with unilateral MD, (eight female; mean age, 55 years; range, 38–71 years), were included in the study. Inclusion criteria were the clinical diagnosis of definite MD according to the guidelines of the American Academy of Otolaryngology Head and Neck Surgery [5] and an age above 18 years. Exclusion criteria consisted of MR-related contraindications such as cardiac pacemakers or claustrophobia, a history of allergies to GBCM and an inability to provide informed consent, as well as middle ear pathology that could impede local contrast uptake.

Contrast agent application

Gadopentetate dimeglumine (Magnograf, Marotrast, Jena, Germany) was diluted eightfold in saline solution and injected intra-tympanically (0.4 ml) under microscopic control. The patients remained in a supine position for a further 30 min with the head turned 45 degrees toward the contralateral side, instructed not to speak or chew during this period. MR imaging was performed 24 hours after application of the contrast agent on a 3 Tesla MR scanner (Magnetom Verio, Siemens Healthcare, Erlangen, Germany), using a commercially available 32-channel head coil (Siemens Healthcare, Erlangen, Germany).

MRI acquisition

We used a Real-IR sequence to differentiate EL from PL and bone and a T2-SPACE sequence to delineate the total inner ear fluid space from the surrounding bone.

T2-SPACE We used a heavily T2-weighted 3D "Sampling Perfection with Application-optimized Contrasts using different flip angle Evolutions" (SPACE) turbo spin echo sequence, with long spin-echo trains with a duration of 477 ms each. The matrix was 384×384 pixels for a field of view of 192×192 mm^2; 56 slices were reconstructed and interpolated to a thickness of 0.5 mm, resulting in a voxel size of 0.5×0.5×0.5 mm^3. Phase oversampling of 100 % and slice oversampling of 14.3 % was applied. Parallel imaging with the GRAPPA algorithm was used with an acceleration factor of two. The echo time (TE) was 135 ms, the repetition time (TR) 1000 ms, the refocusing RF angle 110 degrees, and the receiver bandwidth 283 Hz/pixel. A 90-degree restore pulse was used after each echo train to recover the remaining magnetization. The acquisition was averaged four times to

improve the signal-to-noise ratio (SNR). The resulting total scan time for this sequence was 8:34 min.

3D Real-IR An isotropic 3D real-part reconstruction inversion recovery (Real-IR) turbo-spin echo sequence was acquired, based on the publication by Naganawa et al. [8]. The parameters were: TR 6000 ms, TE 155 ms, TI 1500 ms, fat saturation, constant flip angle of 180 degrees, echo train length of 35, echo train followed by a 90 degree restore pulse, matrix size of 320×320, 36 acquired slices (with 11.1 % slice oversampling), 0.5×0.5 mm^2 in-plane resolution at 0.5 mm slice thickness, receiver bandwidth 195 Hz/pixel, and number of excitations 1. The examination time was 15:14 min.

Image processing

Image Processing (Fig. 1) contained resampling and coregistration of the T2-SPACE volume to the Real-IR volume, Contrast Limited Adaptive Histogramm Equalization (CLAHE), segmentation of the inner ear total fluid space using Random Forest Classification machine learning, fusion of this template with the 3D Real-IR image, endolymph/perilymph segmentation using a Niblack local threshold algorithm, and 3D reconstruction. Details of these procedures are given in the Appendix. Four months after the original image processing algorithm was applied to the raw image data sets of the 16 patients, the procedure was performed again on all raw image data by the same researchers (AB, DK).

Pre-processing

In a first step, we re-sampled the Real-IR and T2-SPACE sequences with cubic interpolation using Analyze 11.0 software (AnalyzeDirect Inc., Kansas City, KN), resulting in a voxel size of 0.1×0.1×0.1 mm^3. The interpolation was done for each voxel by using continuous and smooth cubic polynomials. Coregistration of the T2-SPACE volume to the Real-IR volume was achieved by using a normalized entropy measure for multimodality image alignment [14], incorporated in the image processing software Analyze 11.0. Then, 3D Gaussian and Median filtering 5×5×5 [15] were applied in order to improve the SNR while preserving edges [16]. CLAHE [17] was used to enhance local contrast by performing pixel value equalization on local bases in a 120×120 pixel neighbourhood [18]. This results in an evenly linearized Cumulative Distribution Function (CDF) of grey-scale values within the dynamic range, unveiling areas that are overexposed and underexposed while avoiding overamplification of noise.

Total fluid space segmentation

Generation of the T2-SPACE template, representing the total fluid space of the inner ear, was achieved through interactive segmentation of the T2-SPACE sequence by an ensemble learning classification method named Random Forest (RF) Classification and introduced by Breiman [19], as

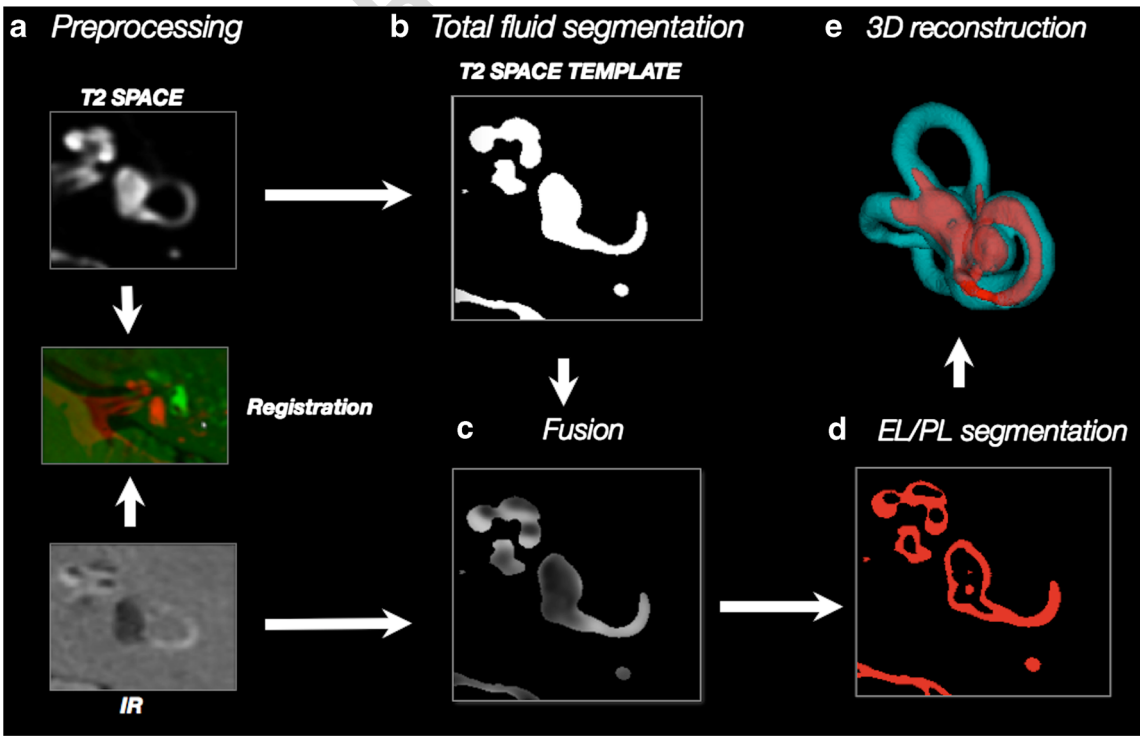

Fig. 1 Workflow of image processing

implemented in the Interactive Learning and Segmentation Toolkit (ILASTIK) [20]. RF combines Breiman's bagging [21] with randomized decision trees proposed by Amit and colleagues [22]. The RF ensemble algorithm consists of a number of unpruned, randomized decision trees, and is capable of capturing highly nonlinear decision boundaries. RF is inherently parallel, fast and robust against noise [23–25]. From the cohort of 16 patients, six patients were randomly selected as the learning data set for this training procedure, which served as a basis for the RF Classifier segmentation of the T2-SPACE sequence in all patients.

Fusion

The external borders of the inner ear in the 3D Real-IR sequence were defined by fusing the previously segmented MR cisternography T2-SPACE template (Fig. 4.2) and the gadolinium-contrasted 3D Real-IR sequence volume (Fig. 4.1). Fusion was performed using the minimum function, Min (T2-SPACE, Real-IR), resulting in a volume termed "Real-IR/T2-SPACE-Temp" (Fig. 1 and Fig. 4.3).

Endolymphatic and perilymphatic space segmentation

The heterogeneous gadolinium contrast medium distribution results in considerable fluctuations of the EL/PL contrast. The small organ size and the relatively low in vivo SNR impedes automated EL/PL segmentation across the inner ear using a global threshold. Therefore, local threshold algorithms (LTA) were used, which adapt the threshold value of each pixel to the local neighborhood characteristics within a defined radius ***r***. The threshold values are spatially determined based on the local image variance [26]. The parameter *R*, introduced by Sauvola and Pietikainen [27], is the maximum value of the standard deviation ($R=128$ for a greyscale image). It can be thought of as a global normalization of the local standard deviation. Trier and Jain found that Niblack local thresholding is one of the best performing local thresholding methods [28]. The Niblack method computes the threshold according to the local mean *m(i, j)* and standard deviation *s(i, j)* for each pixel according to the image characteristics within a window of radius ***r*** around it (AB15) as follows:

$$T(i,j) = m(i,j) + k\sigma(i,j)$$

The size of the local neighbourhood parameter ***r*** should be small enough to preserve local details, but at the same time large enough to suppress noise. The default value for bright phase GBCM enriched perilymph is 0.2 [29]. According to Trier and Jain, a radius of $r=15$ pixels (px) and a bias setting of $k=0.2$ were therefore considered suitable.

In addition, the EL/TFS area ratios of the mid-modiolar cochlear section and the vestibular section were determined by manual selection of ROIs for endolymphatic and perilymphatic spaces (Table 3).

3D Reconstruction

The post-processing included median smoothing ($3\times3\times3$) and separation of the inner ear from the eight cranial nerve / internal auditory meatus using Analyze 11 (3D-Volume Module; AnalyzeDirect Inc., Kansas City, KN). This was done manually by a radiologist and a neurotologist (BEW, RG; both with more than 10 years of experience in temporal bone image evaluation), in a consensus manner. The inner ear was then three-dimensionally reconstructed with different colour codes for the total fluid space and the endolymphatic space.

Four months after the original image processing algorithm was applied to the raw image data sets of the 16 patients, the procedure was performed again on all raw image data by the same researchers (AB, DK). The two calculated sets of data for cochlear and vestibular EL/TFS volume ratios were analyzed for test–retest reliability.

Neurotologic assessment

All patients underwent a neurotologic evaluation including otomicroscopy, audiometry, tympanometry. Cerebellopontine angle tumors were ruled out by i.v. contrast-enhanced T1-weighted cranial MR imaging. Caloric vestibular responses were tested with videonystagmography according to Hallpike [30], the mean maximal slow phase velocity was determined, and the degree of horizontal canal paresis was evaluated according to Jongkees et al. [31]. All patients were diagnosed by two neurotologists with more than 10 years of experience (R.G., E.K.).

Statistical analysis

Test–restest reliability of the semi-automated volumetry and the manual ROI segmentation of cross sections was analyzed using the intra-class correlation coefficient (ICC) and the Pearson correlation coefficient for two trials [32]. The correlation analysis between hearing loss and cochlear EL/TFS ratio was performed with the Pearson correlation coefficient. Statistical analyses were carried out with the IBM SPSS Statistics 20 software (SPSS Inc., Chicago, IL, USA) package.

Results

Clinical characteristics of the study population are summarized in Table 1. The study cohort comprised patients in all stages of Menière's disease. We performed six different LTAs

t1.1 **Table 1** Characteristics of the study population (n=16)

t1.2	Male/female	8/8
t1.3	Age (years)	55 (38–71)
t1.4	Disease duration (months)	91 (3–300)
t1.5	Pure tone average 0.5–3 kHz (dB)	44 (5–120)
t1.6	Canal paresis (%)	36 (2–76)
t1.7	Stage: 1	n=6
t1.8	2	n=3
t1.9	3	n=5
t1.10	4	n=2

Values are expressed as mean (range)

(Fig. 4.4–4.9; Bernsen, Mean, Median, MidGrey, Niblack, Sauvola, [27, 33–37]), comprised of the ImageJ 8-bit Auto Local Threshold plugin [29, 38] on our Real-IR/T2-SPACE-Temp test data sample set (six patients). Niblack's method [39] was least vulnerable to fluctuations of the EL/PL contrast and noise in comparison with other LTA algorithms (Fig. 4). A window radius r=4 px of Niblacks local thresholding algorithm led to many small clusters and over-amplification of noise (Fig. 4.10), whereas a window radius of r=16 px led to cluster agglomeration and loss of details (Fig. 4.12). The intermediate local radius r=8 px performed best across the Real-IR/T2-SPACE-Temp test data sample (Fig. 4.10).

The 3D reconstruction of the inner ear fluid space according to the method described above resulted in a clear delineation of endolymphatic space within the total fluid space in all patients. In general, the endolymphatic space, even in the presence of severe endolymphatic hydrops, could hardly be

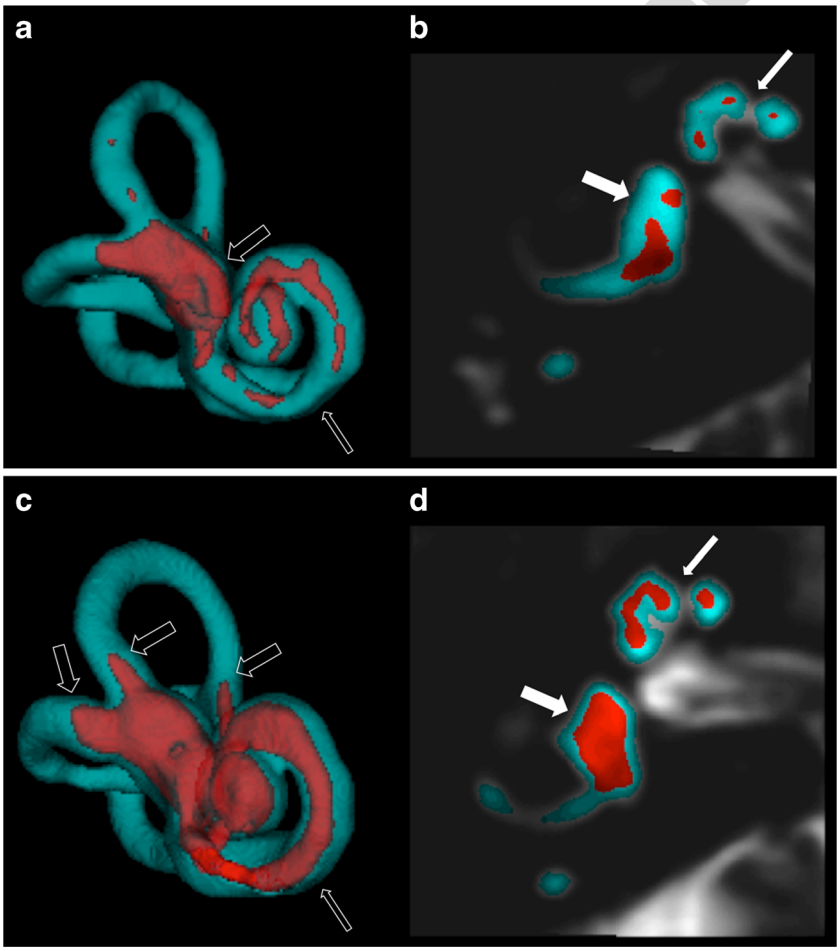

Fig. 2 Locally enhanced inner ear MR imaging (LEIM) of two patients with definite Menière's disease of the right ear after co-registration of T2-SPACE and Real-IR images and automated segmentation of total inner ear fluid space (*cyan*) and endolymph space (*red*). *A* and *C* depict the 3D reconstruction, *B* and *D* depict axial cross-sections. The three semicircular canals are continuously visualized. The interscalar septum is correctly excluded from the inner ear fluid space (*thin filled arrows* in *B* and *D*). *A* and *B* show the right inner ear of a patient with moderate endolymphatic hydrops. The cochlear duct cannot be visualized continuously (*thin transparent arrow*), due to its minute dimensions. The saccular and the utricular subcompartments of the vestibulum are separately depicted (*thick filled arrow*) on the 2D images. *C* and *D* show the right inner ear of a patient with severe endolymphatic hydrops. The cochlear duct is markedly distended and is continuously visualized within all three cochlear turns (*thin transparent arrow).* The saccular and the utricular subcompartments of the vestibulum are confluent (*thick filled arrow*) on 2D images. The herniation of vestibular membraneous labyrinth into the semicircular canals is easily appreciated on the 3D images (*thick transparent arrows*)

visualized within the semicircular canals (Fig. 2a, c). 3D reconstruction in cases with only moderate ELH resulted in discontinuous visualization of the cochlear duct (Fig. 2a), whereas in cases with severe ELH, the cochlear duct is visualized continuously (Fig. 2c). Vestibular endolymphatic space, due to its more spherical geometry and relatively large dimension, is best visualized. While the saccular and the utricular subcompartments are depicted separately on 2D images (Fig. 2b) in cases with moderate ELH, they appear confluent in cases with severe ELH (Fig. 2d). Three-dimensional images depict the delicate shape of the vestibular EL space in cases with moderate ELH (Fig. 2a) and the rather blunt appearance of vestibular EL space in cases with severe ELH (Fig. 2c). Furthermore, the recently described herniation of vestibular membranous labyrinth into the semicircular canals [40] is easily appreciated on 3D images (Fig. 2c). A video rendering of the 3D reconstruction is provided in the appendix.

The results of volumetric measurements of inner ear fluid spaces are summarized in Table 2. The endolymph / total fluid space (EL/TFS) ratio, as a measure for severity of endolymphatic hydrops, was 2–25 %, 15 % (min to max; mean) for the cochlea; and 12–40 %, 28 % (min to max; mean) for the vestibulum. Therefore, a wide range of degrees of endolymphatic hydrops was volumetrically quantified. The cochlear EL/TFS ratio was significantly correlated with hearing loss (Pearson coefficient = 0.747; p=0.001) (Fig. 3).

The results of a second trial of image processing are summarized in Table 3. Test–retest reliability was statistically analyzed for the two primary outcome variables, cochlear EL/TFS volume ratio and vestibular EL/TFS ratio. Both the intra-class coefficient (ICC) and the Pearson correlation coefficient for the EL/TFS volume ratio were 0.99 for both the cochlea and the vestibulum. In contrast, the ICC of the manually segmented EL/TFS area ratios (Table 3) was 0.87 for the cochlea and 0.91 for the vestibulum.

Discussion

More than 150 years after its initial description, MD still represents a major diagnostic and therapeutic challenge. Only recently, the visualization of ELH—as its pathological correlate—has been achieved. Endolymphatic hydrops imaging has been used to link ELH to the deterioration of audiovestibular functions in Menière's disease [41–46]. First

Table 2 Inner ear fluid spaces as measured by Locally enhanced inner ear MR (LEIM) volumetry in 16 patients with definite Menière's disease. The severity of endolymphatic hydrops is expressed as endolymph/total fluid space ratio. Endolymph space within the semicircular canals is too small to be separately visualized by MR imaging; therefore, only the total fluid space of the SCC is listed.

Case No.	Age	PTA (dB)	Canal paresis (%)	Cochlea				Vestibulum				SCC	Inner ear
				Endolymph space (mm^3)	Perilymph space (mm^3)	Total fluid space (mm^3)	EL/TFS ratio (%)	Endolymph space (mm^3)	Perilymph space (mm^3)	Total fluid space (mm^3)	EL/TFS ratio (%)	Total fluid space (mm^3)	Total fluid space (mm^3)
1	64	34	9	9	60	69	13	25	47	72	34	27	169
2	52	20	37	6	66	72	9	12	88	100	12	32	205
3	40	20	42	7	62	68	10	22	74	96	23	42	206
4	52	61	54	19	59	78	25	38	61	99	38	36	212
5	71	90	76	12	44	55	21	25	41	66	38	37	158
6	38	46	6	5	63	68	7	21	70	91	23	44	203
7	50	23	33	11	48	59	18	26	48	74	35	30	162
8	53	15	33	11	50	61	18	22	66	88	25	40	190
9	60	40	40	10	62	72	14	19	53	72	26	31	175
10	71	120	55	21	60	81	25	30	45	75	40	37	193
11	45	5	2	1	56	57	2	14	65	79	18	19	155
12	54	70	54	18	58	76	23	28	52	80	34	35	191
13	55	19	33	5	54	60	9	15	65	80	19	38	178
14	67	60	42	13	52	65	20	23	50	72	31	29	167
15	38	43	19	9	59	67	13	20	49	69	29	29	165
16	67	31	18	10	64	74	13	19	54	74	26	38	186
mean				10	57	68	15	22	58	80	28	34	182
min				1	44	55	2	12	41	66	12	19	155
max				21	66	81	25	38	88	100	40	44	212

PTA = pure tone average at 0.5, 1, 2, 3 kHz; EL/TFS ratio = endolymph/total fluid space ratio; SCC = semicircular canals

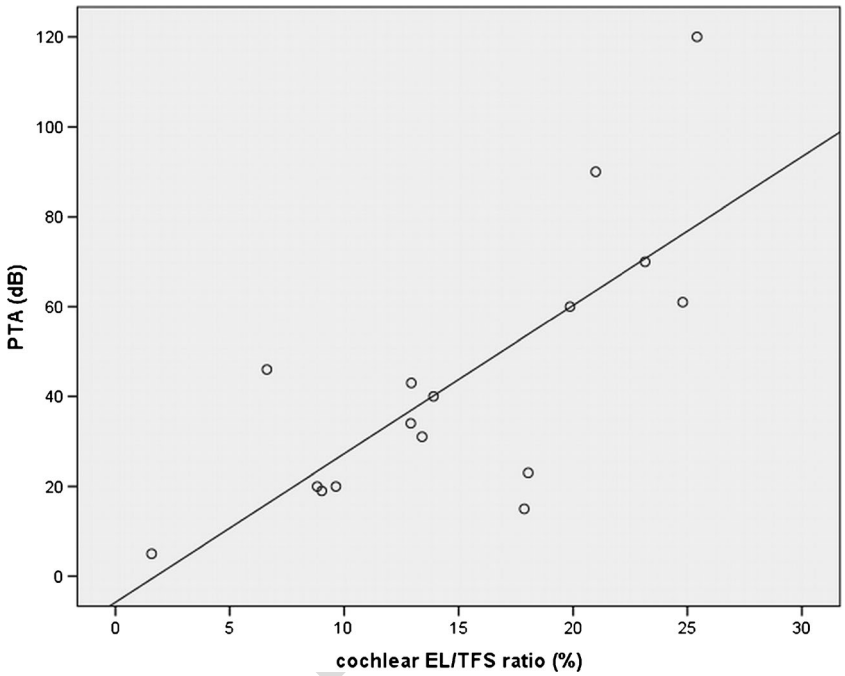

Fig. 3 Correlation between hearing loss, expressed as the four-tone average (PTA) at 0.5, 1, 2, 3 kHz in dB and the cochlear endolymphatic hydrops severity, expressed as the EL/TFS volume ratio

evidence from a cross-sectional study supports the notion that ELH is a morphological phenomenon that progresses with the duration of the disease [41], suggesting that ELH is a valuable disease marker for MD.

Table 3 Test–retest reliability analysis

Case No.	A. Volumetry:						B. Manual ROIs:					
	EL/TFS ratio (%) Cochlea		Difference (%)	EL/TFS ratio (%) Vestibulum		Difference (%)	EL/TFS area ratio (%) Cochlea		Difference (%)	EL/TFS area ratio (%) Vestibulum		Difference (%)
	1st trial	2nd trial		1st trial	2nd trial		1st trial	2nd trial		1st trial	2nd trial	
1	12.9	11.6	10.1	34.3	32.1	6.4	15.8	19.2	17.8	46.6	40.1	14.0
2	8.8	7.3	17.0	12	11.2	7.1	15.9	17.5	9.2	16.9	11.6	31.4
3	9.6	8.6	10.4	23	21.6	6.1	20.5	16.2	21.1	29.0	30.4	4.7
4	24.8	24.8	0.0	38.2	38.5	0.8	29.8	35.4	15.8	53.7	41.3	23.1
5	21	21	0.0	37.7	35	7.2	26.4	36.3	27.3	53.2	55.4	4.0
6	6.6	5.7	13.6	23	21.1	8.3	23.3	20.1	13.8	32.4	38.1	15.0
7	18	16.5	8.3	34.7	30.6	11.8	29.9	33.5	10.9	48.0	44.3	7.7
8	17.9	16	10.6	25.3	25.3	0.0	32.3	25.4	21.2	30.5	26.7	12.3
9	13.9	11.3	18.7	25.8	24.4	5.4	22.3	20	10.3	40.3	41.5	2.9
10	25.4	26.6	4.5	40.4	38.5	4.7	28.8	29.2	1.4	62.0	48.3	22.1
11	1.6	1.3	18.8	17.5	14.3	18.3	1.7	2.3	24.4	19.8	20.8	4.9
12	23.2	23.6	1.7	34.5	33.9	1.7	28.1	34.7	18.9	66.1	60.2	8.9
13	9	8.5	5.6	18.5	17.5	5.4	7.8	10.4	25.4	17.8	25.3	29.6
14	19.9	18.1	9.0	31.5	32	1.6	28.1	22.5	20.1	57.1	42.4	25.8
15	12.9	12.6	2.3	29.2	26.6	8.9	22.2	18.8	15.1	34.3	32.5	5.3
16	13.4	11.9	11.2	26.3	25.2	4.2	26.1	33.3	21.7	30.7	26.2	14.6
mean			8.9			6.1			17.1			14.1

Table 3 .A. Cochlear and vestibular EL/TFS volume ratios from two trials of image processing and the differences (in %). B. Cochlear and vestibular EL/TFS area ratios from two trials of manual ROI segmentation and the differences (in %).

The manual method results in higher test–retest variability

A critical review of the clinical evidence reveals a lack of evidence from controlled trials for the effectiveness of any therapeutic approach towards MD. The strongest evidence is in support of Gentamicine therapy, allowing the statement that it "seems to be an effective treatment" [47–51]. Gentamicine is a destructive treatment aiming for a partial ablation of vestibular functions. It inherently carries a risk of hearing deterioration as a side effect [52]. A therapy with a proven beneficial effect on the natural course of the disease is still lacking. Ideally, a future treatment for Menière's disease should reverse the progression of ELH as its primary pathological feature. A method of objectively quantifying the extent of endolymphatic hydrops is therefore needed. A 3D Real-part Reconstruction Inversion- Recovery sequence with an inversion time of about 1700 ms allowed, for the first time, a separate visualization of endolymph, perilymph and surrounding bone with a single sequence [8]. The delineation between endolymph and perilymph and between endolymph and bone, however, is much more distinct than the contrast between perilymph and bone. This and the variability of contrast uptake [53] render the segmentation between perilymph and bone difficult.

We sought to solve this problem by combining a sequence with excellent demarcation of endolymph from perilymph and bone (3D Real-IR) and a sequence with optimized demarcation between the inner ear fluid space and bone (T2-SPACE). The endolymph signal generated in one sequence was subsequently subtracted from the total inner ear fluid space as defined by the other sequence. Heavily T2-weighted sequences, like CISS or FIESTA, have been used for many years to evaluate the fluid space of the inner ear, e.g., for the diagnosis of inner ear malformations or for the evaluation of

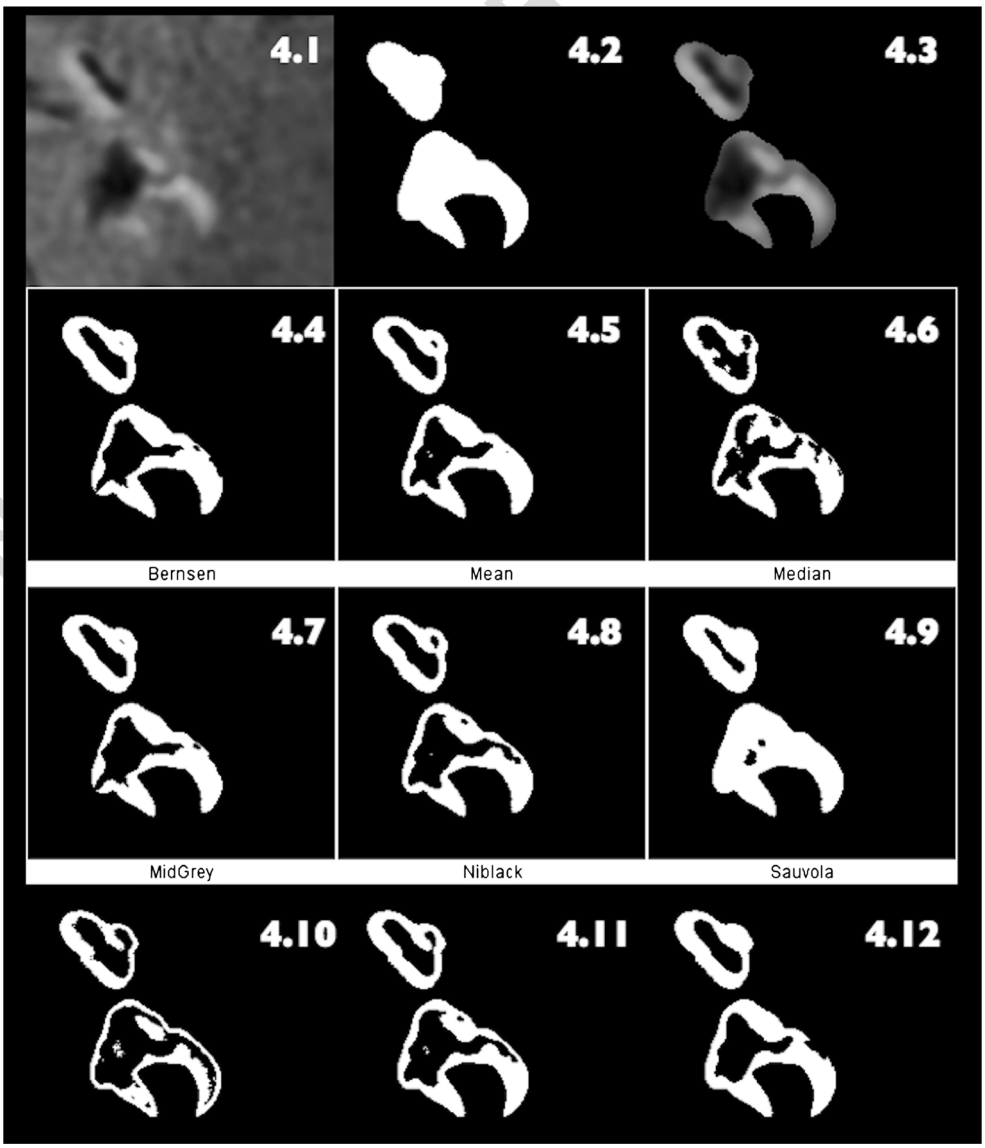

Fig. 4 Comparison of different automated local threshold segmentation algorithms applied to the Real-IR/T2-SPACE-Temp dataset (*4.3*), which results from the fusion of the previously segmented MR cisternography T2-SPACE template (*4.2*) and the gadolinium-contrasted 3D Real-IR sequence volume (*4.1*). The Niblack algorithm (*4.8*) was chosen for the segmentation of enolymph from perilymph space. A window radius of r=8 px was chosen (*4.11*). For comparison, Fig. 4.10 shows segmentation with a window radius of r=4 px, Fig. 4.12 shows segmentation with a window radius of r=16 px

cochlear fibrosis in cochlear implant candidates. These sequences are known to be prone to band-like susceptibility artifacts due to local field heterogeneities that mainly affect the vestibulum and the semicircular canals [54]. Therefore, we used a SPACE sequence to reduce imaging artifacts without significantly increasing the imaging time [55].

We used a Random Forest (RF)-based method to define the outer border of the inner ear fluid space. Numerous studies (e.g., in the fields of dementia research, mammography, preoperative assessment of the femur, or cardiology) have demonstrated the performance of the RF-based systems to be comparable to or to outperform experienced radiologists [56–59].

For the segmentation of EL/PL spaces within the inner ear, the Niblack method [39] performed most effective against fluctuations of the EL/PL contrast and noise in comparison with other LTA algorithms in our hands (Fig. 4), which is in line with the findings of Trier and Jain [28].

Buckingham and Valvassori [60] estimated the average total inner ear fluid volume of the bony labyrinth from histological cross-sections to be 193 mm^3. Average inner ear fluid volumes have been measured by MR volumetric assessments in 29 healthy subjects [61] at 195 mm^3 (range 150–279 mm^3). The authors of this study outlined the borders of inner ear structures manually to obtain a volume. Our 3D-semiautomatic inner ear reconstruction (total fluid space ranged from 155 to 212 mm^3 with an average of 181 mm^3) is consistent with these previously reported data.

Liu et al. [62] used a 3D FLAIR sequence after intratympanic application of GBCM in order to quantify ELH in six MD patients. The mean EL/TFS area ratios were 31 % (range 18–48 %) for the cochlea and 44 % (range 33–58 %) for the vestibulum. The major disadvantage of a FLAIR-based ELH quantification is the limited distinction of endolymphatic space from the surrounding bone. Furthermore, segmentation of EL space was performed manually.

A very recent study [63] presented another approach to quantification of ELH in a sample of patients with various inner ear disorders. These authors also manually drew the outer border of the inner ear fluid space on MR cisternography and fused this region of interest to an i.v. contrast-enhanced 3D Real-IR sequence-like contrast image. Then, endolymph / total fluid space segmentation was performed with a fixed global threshold. The authors reported low inter-observer variability for their method. However, both of these approaches were done on one selected section through the vestibulum and the cochlea only, whereas the 3D volumetric assessment presented here assesses the entire inner ear. I.v. application of GBCM is less invasive than the intratympanic route, at the cost of a lower perilymph signal intensity. Nevertheless, the segmentation method presented here may also be applicable to MR image data obtained after i.v. GBCM application in the future.

Hearing loss in MD patients has been shown to correlate with the severity of cochlear ELH in 2D MR imaging studies [41]. This correlation was not found between semicircular canal paresis and vestibular ELH [64]. In our study, the volumetrically determined cochlear EL/TFS ratio, as an expression of ELH severity, was significantly correlated with hearing loss, supporting the validity of our volumetry method (Fig. 3).

There are limitations to our study that need to be taken into account when interpreting the data. The volumetric method presented here is not exclusively automated, but contains a user-defined input during (1) the interactive Random Forest Classifier based segmentation of the inner ear fluid space, (2) the subdivision of the inner ear into cochlea and vestibulum and (3) the delineation of the inner ear from the internal auditory canal / vestibulocochlear nerve. Nevertheless, we have found excellent test–retest results for our data set, demonstrating that the subjective input to the method is likely to only have a minor effect on the overall results.

Secondly, the volumetric method presented here does not by itself allow the establishment of the diagnosis of MD in an individual patient. For example, patient No. 2 in this series had an EL/TFS ratio of only 2 % in the volumetric evaluation. Despite the clinical diagnosis of definite MD, this patient had only slight functional audiovestibular deficits, most likely due to the early stage in the disease course. Due to the small values for the EL/TFS ratio both in healthy subjects and in the earliest MD disease stage, it may be difficult to define a clear cutoff value between the upper limit of normal variability and the pathologically enlarged EL space in an individual subject, even when larger samples of healthy subjects will be screened with the currently achievable MR image resolution. However, for the purpose of longitudinal volumetric monitoring of ELH during therapeutic studies in MD, this is not necessary, but future studies should investigate this important topic.

In summary, this study for the first time reports an in vivo, computer-aided volumetric quantification of endolymphatic hydrops. By applying the Random Forest Classification machine learning algorithm to MR inner ear cisternography and a Niblack segmentation algorithm to a 3D real reconstruction inversion-recovery sequence, the endolymph / total fuid space was reliably measured over a wide range. This computer-aided volumetric approach is a promising tool to monitor ELH in therapeutic trials in Menière's disease.

Acknowledgments The scientific guarantor of this publication is Robert Gürkov. The authors of this manuscript declare no relationship with any companies whose products or services may be related to the subject matter of the article. This study has received funding by the German Ministry of Research and Education (BMBF). No complex statistical methods were necessary for this paper. Institutional Review Board approval was obtained. Written informed consent was obtained from all subjects (patients) in this study. Methodology: prospective, observational / experimental, performed at one institution.

References

1. Havia M, Kentala E, Pyykko I (2005) Prevalence of Meniere's disease in general population of Southern Finland. Otolaryngol Head Neck Surg 133(5):762–768
2. Alexander TH, Harris JP (2010) Current epidemiology of Meniere's syndrome. Otolaryngol Clin North Am 43(5):965–970
3. Hallpike CS, Cairns H (1938) Observations on the Pathology of Meniere's Syndrome: (Section of Otology). Proc Roy Soc Med 31(11):1317–1336
4. Yamakawa K (1938) Über die pathologische Veränderung bei einem Menière-Kranken. Proceedings of 42nd Annual Meeting Oto-Rhino-Laryngol Soc Japan. J Otolaryngol Soc Jpn 4:2310–2312
5. AAO-HNS (1995) Committee on Hearing and Equilibrium guidelines for the diagnosis and evaluation of therapy in Meniere's disease. American Academy of Otolaryngology-Head and Neck Foundation, Inc. Otolaryngol Head Neck Surg 113(3):181–185
6. Zou J, Pyykko I, Bjelke B, Dastidar P, Toppila E (2005) Communication between the perilymphatic scalae and spiral ligament visualized by in vivo MRI. Audiol Neuro-Otol 10(3):145–152
7. Nakashima T, Naganawa S, Sugiura M et al (2007) Visualization of Endolymphatic Hydrops in Patients With Meniere's Disease. Laryngoscope 117(3):415–420
8. Naganawa S, Satake H, Kawamura M, Fukatsu H, Sone M, Nakashima T (2008) Separate visualization of endolymphatic space, perilymphatic space and bone by a single pulse sequence; 3D-inversion recovery imaging utilizing real reconstruction after intratympanic Gd-DTPA administration at 3 Tesla. Eur Radiol 18(5):920–924
9. Naganawa S, Yamazaki M, Kawai H, Bokura K, Sone M, Nakashima T (2010) Visualization of endolymphatic hydrops in Meniere's disease with single-dose intravenous gadolinium-based contrast media using heavily T(2)-weighted 3D-FLAIR. Magn Reson Med Sci 9(4):237–242
10. Nakashima T, Naganawa S, Pyykkö I et al (2009) Grading of endolymphatic hydrops using magnetic resonance imaging. Acta Otolaryngol 129(s560):5–8
11. Naganawa S, Ishihara S, Iwano S, Sone M, Nakashima T (2010) Three-Dimensional (3D) Visualization of Endolymphatic Hydrops after Intratympanic Injection of Gd-DTPA: Optimization of a 3D-Real Inversion-Recovery Turbo Spin-Echo (TSE) Sequence and Application of a 32-Channel Head Coil at 3 T. J Magn Reson Imaging 31(1):210–214
12. Naganawa S, Yamazaki M, Kawai H, Bokura K, Sone M, Nakashima T (2013) Three-dimensional Visualization of Endolymphatic Hydrops after Intravenous Administration of Single-dose Gadodiamide. Magn Reson Med Sci 12(2):147–151
13. Yamazaki M, Naganawa S, Kawai H, Sone M, Nakashima T (2012) Gadolinium distribution in cochlear perilymph: differences between intratympanic and intravenous gadolinium injection. Neuroradiology 54(10):1161–1169
14. Studholme C, Hawkes DJ, & Hill DL (198) A normalized entropy measure for multimodality image alignment. Proc SPIE Med Imaging (3338):132-143.
15. Iannuccelli E, Mompart F, Gellin J, Lahbib-Mansais Y, Yerle M, Boudier T (2010) NEMO: a tool for analyzing gene and chromosome territory distributions from 3D-FISH experiments. Bioinformatics 26(5):696–697
16. Gonzalez RC, Woods RE (2002) Digital Image Processing. Prentice Hall, Upper Saddle River
17. Zuiderveld K (1994) Contrast limited adaptive histogram equalization. *Graphics gems IV*, ed Paul SH (Academic Press Professional, Inc.), pp 474-485.
18. Pisano ED, Zong S, Hemminger BM et al (1998) Contrast limited adaptive histogram equalization image processing to improve the detection of simulated spiculations in dense mammograms. J Digit Imag 11(4):193–200
19. Breiman L (2001) Random forests. Mach Learn 45:5–32
20. Hamprecht CSaCSaUKaFA (2011) ilastik: Interactive Learning and Segmentation Toolkit. in 8th IEEE International Symposium on Biomedical Imaging (ISBI 2011).
21. Breiman L (1996) Bagging predictors. Mach Learn 24(2):123–140
22. Amit Y, Geman D (1997) Shape quantization and recognition with randomized trees. Neural Comput 9(7):1545–1588
23. Demsar J (2006) Statistical comparisons of classifiers over multiple data sets. J Mach Learn Res 7:1–30
24. Hand DJ, Till RJ (2001) A simple generalisation of the area under the ROC curve for multiple class classification problems. Mach Learn 45(2):171–186
25. Meyer D, Leisch F, Hornik K (2003) The support vector machine under test. Neurocomputing 55(1–2):169–186
26. Sezgin M, Sankur B (2004) Survey over image thresholding techniques and quantitative performance evaluation. J Electron Imaging 13(1):146–168
27. Sauvola J, Pietikainen M (2000) Adaptive document image binarization. Pattern Recogn 33(2):225–236
28. Trier OD, Jain AK (1995) Goal-Directed Evaluation of Binarization Methods. Ieee T Pattern Anal 17(12):1191–1201
29. Anonymous (Image J, Auto Local Threshold (U. S. National Institutes of Health, Bethesda, Maryland, USA).
30. Hallpike CS (1956) The caloric tests. J Laryngol Otol 70(1):15–28 (in eng)
31. Jongkees LB, Maas JP, Philipszoon AJ (1962) Clinical nystagmography. A detailed study of electro-nystagmography in 341 patients with vertigo. Pract Otorhinolaryngol (Basel) 24:65–93 (in eng)
32. Hopkins WG (2000) Measures of reliability in sports medicine and science. Sports Med 30(1):1–15 (in eng)
33. Bernsen J (1986) Dynamic thresholding of gray level images. Proc. Intl. Conf. on Pattern Recognition, pp 1251-1255
34. Davies E (1990) Machine Vision: Theory, Algorithms and Practicalities (Academic Press).
35. Gonzalez R, Woods R (1992) Digital Image Processing. Addison-Wesley Longman Publishing Co., Inc., Boston, MA, USA
36. Chow CK, Kaneko T (1972) Automatic Boundary Detection of Left Ventricle from Cineangiograms. Comput Biomed Res 5(4):388
37. Jain AK (1989) Fundamentals of Digital Image Processing (Prentice Hall)
38. Rasband WS (1997-2012) Image J (U. S. National Institutes of Health, Bethesda, Maryland, USA)
39. Niblack W (1986) An introduction to Digital Image Processing (Prentice-Hall)
40. Gurkov R, Flatz W, Ertl-Wagner B, Krause E (2013) Endolymphatic hydrops in the horizontal semicircular canal: A morphologic correlate for canal paresis in Meniere's disease. Laryngoscope 123:503–506
41. Gurkov R, Flatz W, Louza J, Strupp M, Ertl-Wagner B, Krause E (2012) In vivo visualized endolymphatic hydrops and inner ear functions in patients with electrocochleographically confirmed Meniere's disease. Otology & Neurotology 33(6):1040–1045
42. Gurkov R, Flatz W, Louza J, Strupp M, Ertl-Wagner B, Krause E (2012) Herniation of the membranous labyrinth into the horizontal semicircular canal is correlated with impaired caloric response in Meniere's disease. Otol Neurotol 33(8):1375–1379
43. Gürkov R, Flatz W, Louza JP, Strupp M, Krause E (2011) In-vivo visualization of endolyphatic hydrops in patients with Meniere's disease: correlation with audiovestibular function. Eur Arch Otorhinolaryngol 268:1743–1748
44. Katayama N, Yamamoto M, Teranishi M et al (2010) Relationship between endolymphatic hydrops and vestibular-evoked myogenic potential. Acta Otolaryngol 130(8):917–923

45. Hornibrook J, Coates M, Goh A, Gourley J, Bird P (2012) Magnetic resonance imaging for Meniere's disease: correlation with tone burst electrocochleography. J Laryngol Otol 126(2):136–141
46. Jerin C, Berman A, Krause E, Ertl-Wagner B, Gurkov R (2014) Ocular vestibular evoked myogenic potential frequency tuning in certain Meniere's disease. Hear Res 310:54–59
47. Pullens B, Giard JL, Verschuur HP, & van Benthem PP (2010) Surgery for Meniere's disease. Cochrane Database Syst Rev (1): CD005395
48. Thirlwall AS & Kundu S (2006) Diuretics for Meniere's disease or syndrome. Cochrane Database Syst Rev 3:CD003599
49. James AL, Burton MJ (2001) Betahistine for Meniere's disease or syndrome. Cochrane Database Syst Rev 1, CD001873
50. Phillips JS & Westerberg B (2011) Intratympanic steroids for Meniere's disease or syndrome. Cochrane Database Syst Rev (7): CD008514
51. Pullens B, van Benthem PP (2011) Intratympanic gentamicin for Meniere's disease or syndrome. Cochrane Database Syst Rev 3, CD008234
52. Postema RJ, Kingma CM, Wit HP, Albers FW, Van Der Laan BF (2008) Intratympanic gentamicin therapy for control of vertigo in unilateral Menire's disease: a prospective, double-blind, randomized, placebo-controlled trial. Acta Otolaryngol 128(8):876–880 (in eng)
53. Yoshioka M, Naganawa S, Sone M, Nakata S, Teranishi M, Nakashima T (2009) Individual differences in the permeability of the round window: evaluating the movement of intratympanic gadolinium into the inner ear. Otol Neurotol 30(5):645–648
54. Naganawa S, Koshikawa T, Fukatsu H, Ishigaki T, Fukuta T (2001) MR cisternography of the cerebellopontine angle: comparison of three-dimensional fast asymmetrical spin-echo and three-dimensional constructive interference in the steady-state sequences. AJNR Am J Neuroradiol 22(6):1179–1185
55. Kojima S, Suzuki K, Hirata M, Shinohara H, Ueno E (2013) Depicting the semicircular canals with inner-ear MRI: a comparison of the SPACE and TrueFISP sequences. J Magn Reson Imaging 37(3):652–659
56. Gray KR, Aljabar P, Heckemann RA, Hammers A, Rueckert D (2011) Random Forest-Based Manifold Learning for Classification of Imaging Data in Dementia. Lect Notes Comput Sc 7009:159–166
57. Lempitsky V, Verhoek M, Noble JA, Blake A (2009) Random Forest Classification for Automatic Delineation of Myocardium in Real-Time 3D Echocardiography. Funct Imaging Model Heart, Proc 5528: 447–456
58. Lindner C, Thiagarajah S, Wilkinson JM, Wallis GA, Cootes TF (2013) Fully Automatic Segmentation of the Proximal Femur Using Random Forest Regression Voting. Ieee T Med Imaging 32(8):1462–1472
59. Shili H, Romdhane LB, & Ayeb B (2013) Reliable Probabilistic Classification of Mammographic Masses using Random Forests. in The 9th International Conference on Data Mining (DMIN'2013) (Las Vegas, Nevada, USA)
60. Buckingham RA, Valvassori GE (2001) Inner ear fluid volumes and the resolving power of magnetic resonance imaging: can it differentiate endolymphatic structures? Ann Otol Rhinol Laryngol 110(2): 113–117
61. Kendi TK, Arikan OK, Koc C (2005) Volume of components of labyrinth: magnetic resonance imaging study. OtolNeurotol 26(4): 778–781
62. Liu F, Huang W, Meng X, Wang Z, Liu X, Chen Q (2012) Comparison of noninvasive evaluation of endolymphatic hydrops in Meniere's disease and endolymphatic space in healthy volunteers using magnetic resonance imaging. Acta Otolaryngol 132(3):234–240
63. Naganawa S, Suzuki K, Nakamichi R et al (2013) Semi-quantification of Endolymphatic Size on MR Imaging after Intravenous Injection of Single-dose Gadodiamide: Comparison between Two Types of Processing Strategies. Magn Reson Med Sci 12(4):261–269
64. Kato M, Teranishi M, Katayama N, Sone M, Naganawa S, Nakashima T (2011) Association between endolymphatic hydrops as revealed by magnetic resonance imaging and caloric response. Otol Neurotol 32(9):1480–1485

AUTHOR QUERIES

AUTHOR PLEASE ANSWER ALL QUERIES.

Q1. Please check captured article title, if appropriate.
Q2. Kindly define 'PL'.
Q3. Kindly define 'ROI'
Q4. References 8 and 53 based on original manuscript we received were identical. Hence, the latter was deleted and reference list and citations were adjusted. Please check if appropriate.
Q5. Please check if journal title for Ref# 58 is correct.